Applied Catalysis B: Environmental 184 (2016) 208–215

Contents lists available at ScienceDirect

Applied Catalysis B: Environmental

journal homepage: www.elsevier.com/locate/apcatb

Hopcalite nanoparticle catalysts with high water vapour stability for catalytic oxidation of carbon monoxide

T. Biemelt[a], K. Wegner[a], J. Teichert[a], M.R. Lohe[a], J. Martin[a], J. Grothe[a,*], S. Kaskel[a,b]

[a] Department of Inorganic Chemistry, Dresden University of Technology, Bergstrasse 66, D-01062 Dresden, Germany
[b] Fraunhofer Institute for Material and Beam Technology, Winterbergstrasse 28, D-01277 Dresden, Germany

ARTICLE INFO

Article history:
Received 1 July 2015
Received in revised form 19 October 2015
Accepted 7 November 2015
Available online 10 November 2015

Keywords:
Carbon monoxide oxidation
Flame spray pyrolysis
Hopcalite
Copper manganese oxide
Moisture stable

ABSTRACT

Hopcalite catalysts (copper manganese oxides) with high catalytic activity in CO oxidation catalysis under humid conditions were obtained via flame spray pyrolysis. While commercial hopcalites, for example produced by precipitation methods, immediately deactivate under humid conditions, the new catalysts show significantly reduced deactivation at humidity levels up to 75% and are thus promising materials for personal respiratory protection in respiratory filters for fire fighters and miners. The hopcalite catalysts were obtained by a scalable production route using flame spray pyrolysis (FSP) of mixtures of oleates, 2-ethylhexanoates as well as nitrates dispersed by a surfactant. The textural compositional and also catalytic properties of the FSP-hopcalites were found to be highly tuneable by the type of precursor and the spraying parameters. Adjusting the spraying conditions lead to catalysts with specific surface areas as high as 180 $m^2 g^{-1}$ being mainly composed of $Cu_{1.5}Mn_{1.5}O_4$ by applying 2-ethylhexanoates as precursors. Microemulsions and 2-ethylhexanoates were found to yield hopcalite nanoparticles with very high activity for the catalytic oxidation of carbon monoxide at ambient temperature. The humidity tolerance is attributed to carbon deposits exhibiting a hydrophobic characteristic as indicated by physisorption measurements using water vapour and nitrogen as adsorbates.

1. Introduction

Carbon monoxide is a gas with harmful effects on humans when inhaled already at concentrations as low as 100 ppm [1]. Especially miners, firefighters and soldiers can be confronted with lethal amounts.

An established method to remove CO from breathing air is by equipping respirator masks with an active material causing adsorptive or reactive CO removal. Many catalytically active components such as oxide supported noble metals [2] or transition metal oxides [3] are known to remove CO by catalytic oxidation with atmospheric oxygen at room temperature.

Highly active CO oxidation catalysts were discovered by Haruta et al. who found gold nanoparticles dispersed on α-Fe_2O_3 to be very active even at temperatures as low as −70 °C [4]. However, the high sensitivity of gold based catalysts towards poisoning with organics, poor reproducibility, and rapid ageing is inacceptable for applications in respiratory filters which require stable performance even after long time storage without loss in activity. For this reason, copper manganese mixed oxides known as "Hopcalites" [5] are commercially still the most important catalysts for this application.

Hopcalites with outstanding activity in CO oxidation have been produced by many different synthesis procedures such as sol-gel processes [6], supercritical anti-solvent precipitation [7], redox methods [8], and in the majority of cases co-precipitation [9]. All these routes are based on multiple and partly time consuming preparation steps, such as solving precursors, precipitation, ageing, filtering, washing, drying and calcination. Contamination of the product with sodium ions, which are known to strongly inhibit the catalytic reaction is a common problem [10]. It is also crucial to thoroughly adjust synthesis parameters such as ageing time and calcination temperature for receiving the optimal performing hopcalite catalyst [9,11].

However, one major drawback of hopcalites for the catalytic oxidation of CO is their weak stability against water vapour, inevitably contained in breathing air and stronger adsorbing to the hopcalite surface than oxygen or carbon monoxide, thus poisoning its catalytic properties [12].

* Corresponding author. Fax: +49 351 46337287.
E-mail addresses: tim.biemelt@chemie.tu-dresden.de (T. Biemelt), karl.wegner@chemie.tu-dresden.de (K. Wegner), Johannes.teichert@chemie.tu-dresden.de (J. Teichert), Martin.Lohe@chemie.tu-dresden.de (M.R. Lohe), jan.martin@chemie.tu-dresden.de (J. Martin), julia.grothe@chemie.tu-dresden.de (J. Grothe), Stefan.kaskel@chemie.tu-dresden.de (S. Kaskel).

http://dx.doi.org/10.1016/j.apcatb.2015.11.008
0926-3373/

Table 1
Sample codes and synthesis conditions.

Sample[a]	Solvent[b]	Mn:Cu (mol mol^{-1})	c_{metal} (M)	$O_{2,disp.}$ (L min^{-1})	LF[c] (mL min^{-1})
o-1	H	0.0	0.05	4.89	3.0
o-2	H	1.0	0.05	4.89	3.0
o-3	H	2.0	0.05	4.89	3.0
o-4	H	5.0	0.05	4.89	3.0
o-5	H	7.0	0.05	4.89	3.0
o-6	H	14.0	0.05	4.89	3.0
o-7	H	19.0	0.05	4.89	3.0
o-8	H	∞	0.05	4.89	3.0
e-1[com]	E	2.0	0.18	5.00	5.0
e-2[com]	E	2.0	0.10	5.00	2.5
e-3[com]	E	2.0	0.05	5.00	2.5
e-4[com]	E	2.0	0.05	7.50	2.5
e-5[com]	E:EHA = 1	2.0	0.05	5.00	2.5
e-6[com]	E:M = 1	2.0	0.05	5.00	2.5
e-7[com]	E:M = 0.5	2.0	0.05	5.00	2.5
e-8[com]	M:A = 15.7	2.0	0.05	5.00	2.5
e-9[com]	M:A = 15.7	2.0	0.05	7.50	2.5
e-10[ih]	M:A = 15.7	2.0	0.05	7.50	2.5
e-11[ih]	M:A = 15.7	2.8	0.05	7.50	2.5
e-12[ih]	M:A = 15.7	2.4	0.05	7.50	2.5
m-1	Hep	2.0	0.10	7.50	2.5
m-2	Hep	2.0	0.05	7.50	2.5

[com] Commercial Mn(II)-2-ethylhexanoate was used.
[ih] In house made Mn(II)-2-ethylhexanoate was used.
[a] o = oleates, e = 2-ethylhexanoates, m = microemulsion.
[b] H = *n*-hexane, E = ethanol, EHA = 2-ethylhexanoic acid, M = methanol, A = acetic acid, Hep = *n*-heptane.
[c] LF = liquid feed.

Hence, a hopcalite production route with reduced number of synthesis steps, contaminant free metal oxide sources and increased product stability against moisture is highly desirable in terms of economic production time and improved environmental friendliness, especially concerning the absence of waste water and, more important, durability of the catalyst itself.

A useful approach of mixing metal ions on the atomic level for the production of doped and mixed oxides is a process named flame spray pyrolysis (FSP) [13]. It is characterised by generating combustible aerosols with droplets smaller than 5 μm in diameter, containing volatile and/or combustible metal precursors dissolved in an organic fuel. Ignition leads to instantaneous evaporation and generation of solvent free nanoparticles within the flame [14]. Several binary and mixed oxides, as well as composites have been synthesised with FSP and were found to outperform their more traditional e.g., co-precipitated counterparts in numerous applications. Moreover, FSP is an established scalable process used industrially for nanoparticle production. A comprehensive summary was given by Teoh et al. [15].

Here we consider three different types of precursors for the FSP-synthesis of hopcalite, namely mixtures of (i) oleates, (ii) 2-ethylhexanoates, and (iii) nitrates dispersed with the help of a surfactant. In addition we demonstrate high catalytic activities of FSP derived hopcalites. A correlation between activity in CO-oxidation and particle characteristics derived from nitrogen and water physisorption, elemental analysis, electron microscopy and X-ray powder diffraction is conducted.

2. Experimental

2.1. Syntheses of precursors

2.1.1. Mn(II)/Cu(II) mixed oleate precursors

Mixed manganese/copper oleates were synthesised from sodium oleate and the metal chlorides. $CuCl_2{\cdot}2H_2O$ (Alfa Aesar 99%) and $MnCl_2{\cdot}2H_2O$ (Grüssing 99%) were dissolved in a 1:1 volume mixture of ethanol and water to give an overall metal concentration of 0.6 M. Subsequently, twice the volume of a suspension of 0.6 M sodium oleate (Sigma–Aldrich ≥ 82%) in *n*-hexane (Merck p.A.) was added and refluxed at 70 °C for 4 h. Afterwards, the separated ion-exchanged organic phase was washed twice using half its volume of water. Finally it was diluted with *n*-hexane to 0.05 M overall metal concentration resulting in a clear solution with the colour varying between brown and green depending on copper/manganese ratio.

2.1.2. Mn(II)-2-ethylhexanoate

15.0 g $MnCO_3$ (Sigma–Aldrich 99.9%) were suspended in a mixture of 100 g 2-ethylhexanoic acid (abcr 99%) and 100 g deionised water. The mixture was refluxed at 110 °C for 24 h to react to a clear water and a dark red organic phase, which were then severed using a separating funnel.

2.1.3. Mn(II)/Cu(II) mixed 2-ethylhexanoate precursors

In general commercial Cu(II)-2-ethylhexanoate (Sigma–Aldrich 98%) and in house made or commercial Mn(II)-2-ethylhexanoate (abcr/Alfa Aesar 40 wt% in mineral spirits) were dissolved in different solvents resulting in overall metal concentrations of 0.05 M to 0.18 M with Mn:Cu molar ratios ranging from 2.0 to 2.8. Details on the precursors produced from 2-ethylhexanoates are given in Table 1.

2.1.4. Inverse microemulsion precursors

Aiming at the formation of preferably small micelles we took our previous findings [16] and the work of Henle et al. [17] as a reference. 8.57 M (m-1) and 4.29 M (m-2) solutions of $Mn(NO_3)_2{\cdot}4H_2O$ (abcr 98%): $Cu(NO_3)_2{\cdot}3H_2O$ (abcr 98%) = 2.0 mol mol^{-1} in 5.70 g deionised water were dispersed in a mixture of 281.24 g *n*-heptane and 69.06 g nonylphenol polyethylene glycol ether (5 EO) MARLOPHEN NP 5 (SASOL) by ultra-sonication to give overall metal concentrations of 0.10 M and 0.05 M for m-1 and m-2, respectively.

2.2. Flame spray pyrolysis

The different precursor solutions were fed through a commercial nozzle (NPS10, Tethis) with liquid feed rates ranging from 2.5 to 5.0 mL min^{-1} ignited by a surrounding supporting-flame to pre-

vent the main flame from self-extinguishing. The supporting-flame gas flow consisted of 1.50 L min^{-1} CH_4 and 3.00 L min^{-1} O_2. The liquid feed was delivered by a micro annular gear pump (mzr-2905, HNP Mikrosysteme GmbH) and dispersed by 4.89 to 7.50 L min^{-1} O_2 with a dispersion gas pressure drop accounting to 2.0 bar adjusted by a displaceable annular gap encircling the liquid feed capillary. All gas flows were controlled by thermal mass flow controllers (Bronkhorst). The synthesised black voluminous powders were collected by a binder-less glass fiber filter (GF/A Whatman) with the help of a rotary vane pump (Vacuubrand RZ 9). All gases had a purity of 99.999% and were purchased from Air Liquide. The specific synthesis conditions for each sample are listed in Table 1.

2.3. Characterisation

X-ray powder diffraction patterns were collected in three ranges per sample in reflection mode with a PANalytical X'Pert Pro diffractometer using Cu Kα_1 radiation. A step size of 0.013° 2θ was applied and the ranges were added and compared to reference data from the ICDD powder diffraction data base, which are referenced by the respective powder diffraction file (PDF) numbers. Applying the SCHERRER-method to all diffraction peaks of $Cu_{1.5}Mn_{1.5}O_4$ in the range of 10 to 70° 2θ, hopcalite crystallite sizes were calculated.

Nitrogen physisorption isotherms were recorded with a Quantachrome NOVA 4000 at −196 °C after activating the samples at 150 °C for 12 h in dynamic vacuum. The specific surface area (S_{BET}) was determined by applying the multi-point BET-method in the range of p/p_0 = 0.05–0.20. Water physisorption was conducted at 25 °C with a Quantachrome HYDROSORB 1000 after activating the samples in the abovementioned way.

Scanning electron micrographs were obtained using a DSM-982 Gemini (Zeiss) operating at 6 kV. Prior to the measurements the samples were fixed on an adhesive carbon pad and sputtered with gold to provide the necessary electrical conductivity. For EDX measurements the acceleration voltage was set to 20 kV. Further elemental analyses (CHNS) were carried out with a EuroEA CHNS-O elemental analyser.

Dynamic light scattering was performed using a Zetasizer Nano ZS (Malvern Instruments). The micelle sizes of m-1 and m-2 were determined at 20 °C. Kinematic viscosities of the microemulsions were measured with an efflux viscosimeter and converted into dynamic viscosities by using the liquid density detected with a pycnometer. Average micelle diameters (z-average) were calculated from intensity weighted size distributions with the NNLS-algorithm.

Catalytic tests were performed in a fixed bed tubular reactor (d_{in} = 6 mm) equipped with two NDIR-sensors smartModul^{PREMIUM} (Pewatron) for the simultaneous determination of CO and CO_2 concentrations in the exhaust gas stream. The temperature was monitored inside the catalyst bed by a thermocouple inserted in a glass capillary. In a typical setup, 100 mg of catalyst were exposed to a gas mixture consisting of 0.67 vol.% CO, 66.00 vol.% N_2, and 33.33 vol.% O_2 (4 L h^{-1}) for at least 20 min at each temperature. Catalyst activation was conducted by heating to 300 °C in a N_2 stream of 3 L h^{-1} and switching to O_2 (1 L h^{-1}) after 10 min, holding the temperature for additional 50 min. CO and CO_2 signals were recorded in the exhaust gas during the activation procedure. For testing under humid conditions, the gas stream was saturated with water vapour by flowing through a reservoir containing deionised water at 15 °C. A humidity of 75% RH at 20 °C was simulated in this way.

Conventional pressing of the particles with p = 200 MPa led to nearly complete loss of porosity. In order to guarantee sufficient gas permeability through the catalyst bed, the as received voluminous hopcalite powders were dispersed in water and densified by centrifugation. Subsequent drying, grinding and sieving, gave grain sizes of 125–250 μm that were used for the catalytic tests.

Temperature dependent desorption of H_2O, CO and CO_2 was monitored using a NETZSCH STA 409 Luxx equipped with a mass spectrometer (NETZSCH QMS 403 Aëolos) in synthetic air (100 mL min^{-1}) between ambient temperature and 500 °C with a ramp of 10 K min^{-1}.

3. Results and discussion

3.1. Structural and textural properties of the hopcalites

Three different types of precursor solutions were evaluated for their ability to generate hopcalite nano particular powders via FSP aiming at high activity in the catalytic oxidation of carbon monoxide at ambient temperature under dry and humid conditions. Their textural properties and compositions are listed in Table 2.

3.1.1. Oleates

Oleates were chosen as precursors because of the good availability of oleic acid and their very similar decomposition onset temperatures of 248 °C and 275 °C for pure Cu(II)- and Mn(II)-oleate, respectively, as confirmed by thermo-gravimetric measurements, plotted in Fig. S1. These narrow decomposition onset temperatures lead to powders without segregation of single oxide species as nearly the same amount of energy is required to initiate the combustion process within the spray flame.

By varying the ratio of these two oleates, different oxide samples were obtained concerning their manganese and copper content. By applying pure Cu(II)-oleate, black crystalline CuO nanoparticles with 32 nm crystallite size were synthesised (o-1 in Fig. S2). Processing a solution of pure Mn(II)-oleate resulted in a mixture of nano-crystalline Mn_2O_3 and Mn_3O_4 (o-8) determined by X-ray powder diffraction. Nano particular mixed-oxide powders, derived from feeding mixtures of Cu(II)- and Mn(II)-oleate solutions to the FSP-process, consisted of $Cu_{1.5}Mn_{1.5}O_4$ and Mn_3O_4, showing a strong dependence of mass fractions on the initial Mn:Cu-ratio. No crystalline CuO impurities were found in these samples.

N_2-physisorption experiments resulted in IUPAC type II isotherms [18] indicating the presence of nanoparticles and yielding specific surface areas ranging from 35 m^2 g^{-1} to 91 m^2 g^{-1} (Table 2) for the pure CuO sample o-1 and the Mn:Cu = 5 mol mol^{-1} mixed sample o-4, respectively.

EDX investigations showed that all of the oleate based samples contained small amounts of sodium (Table 2), most likely originating from the synthesis of the oleate compounds itself that utilised commercially available Na-oleate as a starting material. We were not able to extract excess sodium ions neither from the Mn-Cu mixed oleates, nor the final products o-1 to o-8, even though they have been intensively washed with deionised water. Sodium ions were shown to inhibit the catalytic conversion of CO to CO_2 to some extent [10], therefore it is of great importance to synthesise sodium free hopcalite catalysts.

3.1.2. Mn(II)- and Cu(II)-2-ethylhexanoates

As an alternative, sodium free Mn(II)- and Cu(II)-2-ethylhexanoates were used to generate a second type of precursor solutions. The influence of precursor concentration, dispersion oxygen gas flow and liquid precursor flow on the resulting hopcalite nanoparticles was investigated, especially optimizing the resulting porosity with the aim to yield isolated mixed-oxide crystallites as small as possible in diameter. For a starting point, a composition of Mn:Cu = 2 mol mol^{-1} was chosen, as the same composition ranges among the materials with the highest specific surface areas synthesised from the presented oleate precursors and simultaneously is known to exhibit the highest catalytic activity in Mn-Cu-O systems [11].

Table 2
Textural properties and compositions of FSP derived hopcalites and the commercial reference material Carulite 300.

Sample[a]	S_{BET}[b] ($m^2\ g^{-1}$)	d_{BET}[c] (nm)	d_{cryst}[d] (nm)	Mn:Cu[e] (mol mol^{-1})	C[f] (wt%)	Na, P[e] (at%)
o-1	35	26.4	31.9	0	0.37	5.1^{Na}
o-2	76	14.0	–	1.09	0.11	4.3^{Na}
o-3	80	13.8	–	1.68	0.09	3.6^{Na}
o-4	91	13.2	–	5.46	0.08	3.6^{Na}
o-5	74	16.2	–	7.81	0.05	4.7^{Na}
o-6	80	15.4	–	14.96	0.07	4.3^{Na}
o-7	74	16.7	–	20.51	0.08	2.6^{Na}
o-8	54	23.6	–	∞	0.04	3.0^{Na}
e-1	35	31.5	13.2	2.20	–	7.2^{P}
e-2	113	9.7	6.2	1.79	–	7.6^{P}
e-3	136	8.1	5.4	1.82	–	7.8^{P}
e-4	163	6.8a	4.6	1.86	–	8.4^{P}
e-5	106	10.4	11.4	1.80	–	8.0^{P}
e-6	155	7.1	9.1	1.77	–	7.8^{P}
e-7	160	6.9	9.7	1.51	–	6.2^{P}
e-8	156	7.1	8.7	1.75	–	7.0^{P}
e-9	182	6.1	7.4	1.77	–	7.0^{P}
e-10	164	6.7	8.5	1.80	0.24	$0.0^{P,Na}$
e-11	128	8.6	7.9	2.46	0.46	$0.0^{P,Na}$
e-12	160	6.9	7.9	1.95	0.31	$0.0^{P,Na}$
m-1	97	11.3	10.8	1.96	0.13	$0.0^{P,Na}$
m-2	114	9.6	10.9	1.93	0.11	$0.0^{P,Na}$
Carulite 300	310	3.6	–	2.30	0.12	1.4^{Ca};0.7^{K}

(–); not determined.
[P] at% phosphor, [Na] at% sodium, [Ca] at% calcium, [K] at% potassium.
[a] Precursor type: o = oleate, e = 2-ethylhexanoate, m = microemulsion.
[b] Derived from nitrogen physisorption with multipoint BET analysis at p/p_0 = 0.05–0.20.
[c] Calculated from Eq. (1).
[d] Derived from SCHERRER-equation.
[e] Detected by EDX.
[f] Determined by combustion method with CHNS-Analyser.

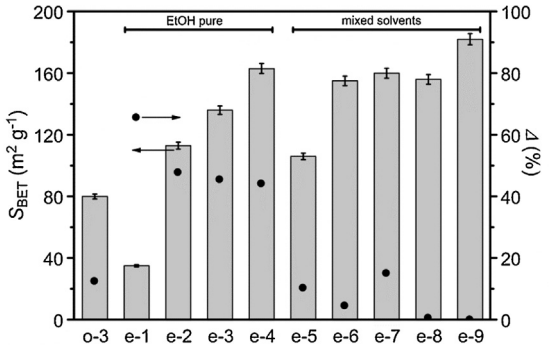

Fig. 1. Specific surface areas and deviation Δ between d_{BET} and d_{cryst} (Eq. (2) in text) depending on synthesis conditions for 2-ethylhexanoates as FSP hopcalite precursor.

The results of varying spraying conditions are summarised in Fig. 1. Specific surface areas of FSP oxide particles in general mainly depend on the precursor concentration and the residence time in the flame [19]. Thus, the trends observed can be explained as follows. Decreasing the precursor concentration (e-1, e-2 and e-3), results in less primary particles, depressing coagulation effects because of fewer hits among particles passing the high temperature region of the flame. The same effect can be achieved by decreasing the feed rate of the liquid precursor and is additionally strengthened by adjusting both parameters simultaneously (e-2, e-3). Increasing the oxygen dispersion gas flow from 5.0 to 7.5 L min^{-1} (e-3 to e-4), results in a hopcalite nano-powder with further increased specific surface area. One possible reason for that observation is the accelerated velocity through the flame, preventing the forming particles from intensive sintering. Additionally the flame temperature is reduced, as the heat of reaction of exothermic combustion of the precursor solution is dissipated by higher flows of ambient temperature oxygen gas as compared to the reference samples e-1 and o-4.

For precursor concentrations not exceeding 0.1 M, the combustion temperature is mainly influenced by the type of organic solvent (fuel) used. Thus, flame temperature and sintering of the particles can also be influenced by varying the solvent composition. Choosing methanol and acetic acid as solvent components directly lowers the flame temperature, by attenuating the overall combustion enthalpy of the precursor system, as compared to pure ethanol (e-1 to e-4). Applying a mixture of 94 vol.% methanol and 6 vol.% acetic acid, a dispersion oxygen gas flow of 7.5 L min^{-1} and a precursor concentration of 0.05 M resulted in sample e-9 with a specific surface area as high as 182 $m^2\ g^{-1}$. In contrast, increasing the combustion enthalpy of the solvent by using 2-ethylhexanoic acid as a co-compound besides ethanol (e-5) led to a significantly reduced specific surface area as compared to sample e-4 derived from pure ethanol.

Spraying conditions of samples e-4 and e-9 resulted in nanopowders, exhibiting nearly equal specific surface areas (d_{BET} = 6.8 and 6.1 nm for e-4 and e-9, respectively). Nevertheless, calculating the relative deviation Δ between the geometrically derived mean particle diameter d_{BET} and the crystallite size d_{cryst}, (calculated from XRD measurements by applying the SCHERRER-equation to all diffraction peaks accounting to $Cu_{1.5}Mn_{1.5}O_4$) with

$$d_{BET} = \frac{6}{\left(S_{BET} \times \rho_{Cu_{1.5}Mn_{1.5}O_4}\right)} \quad (1)$$

assuming spherical particles and

$$\Delta = \frac{\sqrt{\left(d_{BET} - d_{cryst}\right)^2}}{d_{BET}} \times 100 \quad (2)$$

led to surprisingly different values. All samples originating from simply ethanol containing precursor solutions (e-1 to e-4) exhibit an increased Δ (Fig. 1, secondary y-axis), which can be interpreted as samples containing particles composed of inter-grown hopcalite crystallites. Changing to mixed ethanol based solvent composi-

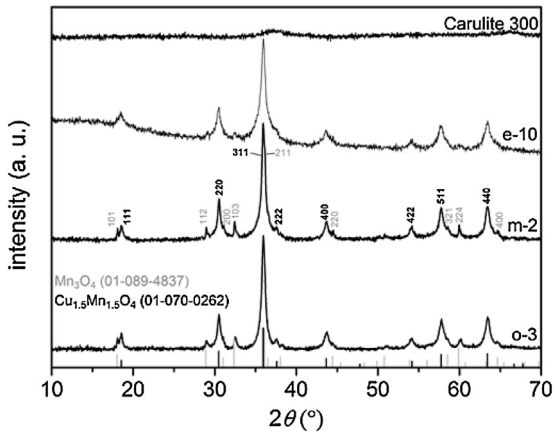

Fig. 2. X-ray powder patterns of representative samples prepared with different precursor solutions, having comparable Mn:Cu molar ratios.

tions (e-5 to e-7), resulted in decreased Δ values. Further solvent exchange to methanol based compositions for samples e-8 and e-9, lead to $\Delta \approx 0$, representing truly separated hopcalite single crystal particles, which are favourable for the catalytic application as the available reactive surface is maximised.

The hopcalite nanopowders obtained by optimising the specific surface area and generating separated single crystals of $Cu_{1.5}Mn_{1.5}O_4$ were invariably found to contain phosphorus in concentrations as high as 8 at% by EDX measurements. Infrared spectroscopic investigations of the separately calcined Cu(II)- and Mn(II)-2-ethylhexanoate educts (Fig. S3) revealed commercial Mn(II)-2-ethylhexanoate as its origin. An explanation for the undesired phosphorus impurity from the manufacturer was not available upon request.

To prevent our particles from containing phosphorus, which we found acting as a poison for mixed manganese copper oxide catalysts in the oxidation of carbon monoxide, Mn(II)-2-ethylhexanoate was synthesised in house by reacting $MnCO_3$ with an excess amount of 2-ethylhexanoic acid. For the FSP process the optimised spraying conditions were used, varying only the initial Mn:Cu-ratio and yielding samples e-10 to e-12 by applying the fresh manganese precursor. Their textural properties are close to those of the optimised sample e-9 concerning their specific surface areas of up to 164 $m^2\,g^{-1}$ for e-10 and can be found in Table 2. EDX measurements confirmed the expected absence of phosphorus in these samples.

Fig. 2 contains the X-ray powder diffraction pattern of sample e-10, which is representative for all samples derived from 2-ethylhexanoates via FSP. The nano particular powders are composed of cubic spinel $Cu_{1.5}Mn_{1.5}O_4$ as the main crystalline phase, besides small amounts of tetragonal Mn_3O_4 (hausmannite) in some samples.

From a precursor composition site of view $CuMn_2O_4$ should crystallise as the main phase, which however was not found in our samples. The reason for that observation is most likely the temperature distribution within the spray flame, causing rapid heating of the precursor solution and leading to fast evaporation and nanoparticle formation while passing through very sharp temperature gradients. These are responsible for cooling the nanoparticles rapidly, after leaving the hot flame, as well [20]. Temperature quenching of solid state reactions in the Mn-Cu-O-system is known to preferentially yield the metastable spinel $Cu_{1.5}Mn_{1.5}O_4$ [21], confirming the special temperature conditions within the FSP process and giving an explanation for yielding Mn_3O_4 as a by-product. Further descriptions of reasons for slight inconsistency in particle morphology concerning a bimodal particle size distribution with few spheres in the range of 100 nm as can be seen from SEM micrograph of sample e-10 in Fig. S4 are given in Section 3.1.3 and in our previous investigations [16]. Here a similar mechanism leads to a bimodal particle size distribution.

Comparing these results to the final Mn:Cu-ratio derived from EDX measurements (listed in Table 2), leads to the assumption that a manganese rich, X-ray amorphous phase has to be present in the samples e-1 to e-12, as well, since Mn:Cu was found to be >1.5 mol mol^{-1} for each sample (Table 2). The particle size of this amorphous phase is probably smaller than the crystallite size d_{cryst} determined for cubic spinel phase $Cu_{1.5}Mn_{1.5}O_4$ due to the fact that especially for samples e-5 to e-12 the specific surface area derived mean particle diameter d_{BET} is smaller than d_{cryst} (Table 2). Hence, a distinct part of the overall specific surface area might originate from the X-ray amorphous phase.

Since a polydisperse particle size distribution is observed in the scanning electron micrographs of representative sample e-10 in Fig. S4, the values derived for d_{BET} should be understood as an approximation. Nevertheless, the powder is mainly composed of slightly agglomerated nanoparticles with an approximate size of 10 nm in diameter as confirmed by SEM and TEM micrographs, shown in Fig. 3a and c, respectively.

3.1.3. Inverse microemulsions

An alternative to carboxylate precursors for FSP are inverse microemulsions, as it is feasible to dissolve inexpensive nitrate metal salts in sufficiently high concentrations in a non-polar solvent (fuel) and at the same time forming hopcalite nanoparticles smaller than 15 nm in diameter [16].

Two different metal salt concentrations having the molar ratio Mn:Cu = 2 mol mol^{-1} within the water containing micelles were applied, leading to samples m-1 and m-2. Both inverse microemulsions were found to contain micelles with 4.7 nm in diameter by dynamic light scattering investigations, taking into account the different viscosities and refractive indices, which are listed in Table S1. The different initial concentrations lead to powders with specific surface areas as high as 97 and 114 $m^2\,g^{-1}$ for sample m-1 and m-2, respectively (Table 2). A bimodal particle size distribution was observed during (S)TEM and SEM investigations, with a main fraction of around 10 nm and some larger spherical particles up to 100 nm in diameter (see Fig S5). The amount of larger spheres was found to be increased for m-1, which is consistent with the slightly reduced specific surface area as compared to sample m-2. These two types of particles, which were contained in the samples generated from 2-ethylhexanoates, as well, originate from different formation mechanisms within the spray flame. On the one hand, precursor evaporation and subsequent vapour combustion occurs to form small mono-disperse nanoparticles. On the other hand, precipitation of the precursor on the aerosol droplet surface and subsequent calcination resulting in poly-disperse, micron-sized and sometimes hollow spheres is possible. It occurs if the energy of the flame transferred to the precursor solution is reduced compared to pathway one [22]. For catalytic applications the first formation pathway is preferred, because the catalytically available surface area for those particles is up to two orders of magnitude higher.

Both samples consist of a mixture of the cubic spinel $Cu_{1.5}Mn_{1.5}O_4$ as the main phase and tetragonal Mn_3O_4 as a minor component, as confirmed by X-ray powder diffraction (see Fig. 2).

3.2. Catalytic properties

3.2.1. Oleates

Oleate derived hopcalite particles, showed no significant activity at room temperature for the oxidation of carbon monoxide, even after activation in oxygen. Raising the reactor temperature to 150 °C resulted in some catalytic activity, strongly depending on the molar composition of the catalysts. These results are summarised in Fig.

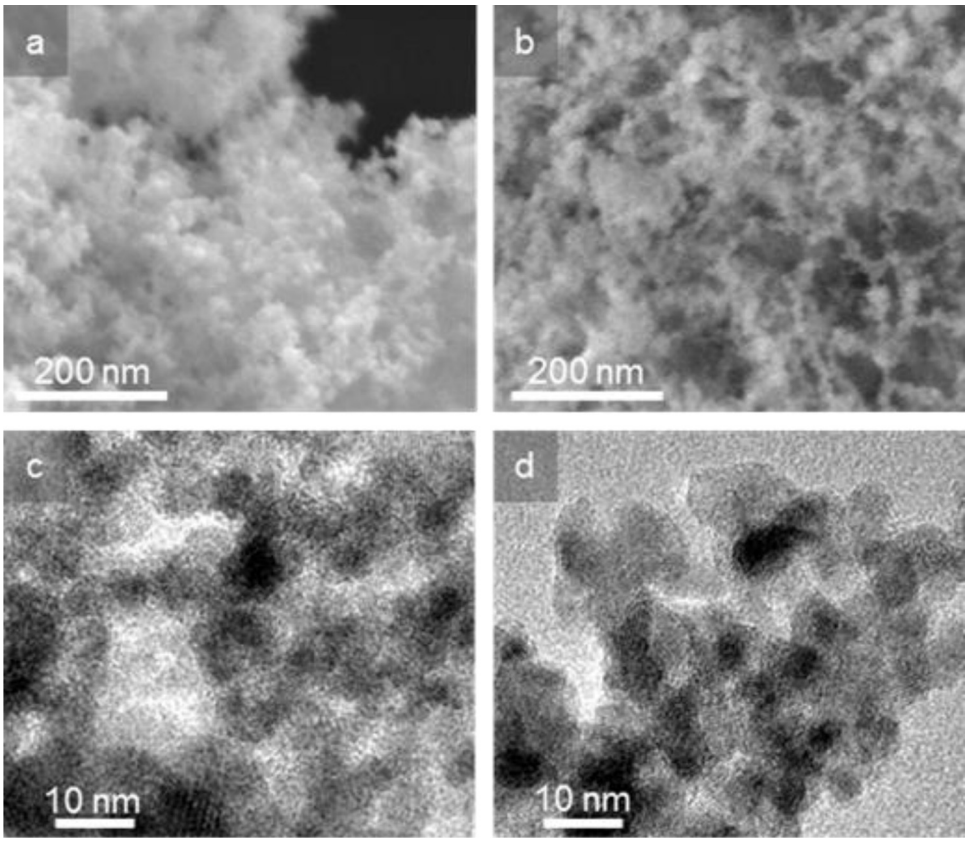

Fig. 3. SEM (a,b) and TEM (c,d) micrographs of samples e-10 (a,c) and m-2 (b,d).

S6. Sample o-3 with an initial ratio of Mn:Cu = 2 mol mol^{-1} showed the best performance with approximately 80% CO conversion. This Mn:Cu-ratio has been reported being the optimal composition for the catalytic oxidation of carbon monoxide [11]. However, those previously published catalysts were already active at ambient conditions. A possible reason for the high temperatures needed to observe CO conversion is the amount of sodium in the respective samples ranging from 2.6 to 5.1 at% for sample o-7 and o-1, respectively. Sodium is known for poisoning the catalyst and therefore strongly inhibiting the catalytic reaction [10].

3.2.2. Mn(II)- and Cu(II)-2-ethylhexanoates

2-ethylhexanoate based materials show diverse behaviour. While the phosphorus contaminated hopcalite powders, synthesised from commercially available Cu(II)- and Mn(II)-2-ethylhexanoate (Alfa Aesar, abcr) were found to be nearly inactive at ambient conditions, the phosphorus free samples e-10, e-11 and e-12 were active at room temperature. Sample e-12 exhibiting a Mn:Cu-ratio of 1.95 mol mol^{-1} shows high conversions up to 60% as illustrated by Fig. 4. Increasing and decreasing the Mn:Cu-ratio resulted in decreasing conversion levels, in analogy to the results obtained for the oleate precursors (Fig S6). Sample e-12 nearly shows the same performance as the reference material Carulite 300, which was activated in oxygen at 300 °C prior to testing, as well. Non activated Carulite 300 and sample e-12 allowed conversions of CO ranging around 20% and 50%, respectively. During inert activation of the commercial catalyst carbon dioxide could be detected, originating from left over carbonate species or physisorbed molecules possibly blocking the active sites. Activation of e-12 however released no carbon dioxide under inert conditions but switching to pure oxygen atmosphere at 300 °C resulted in signals for carbon dioxide as well as carbon monoxide. Most likely these signals originate from oxidative removal of carbonaceous residues.

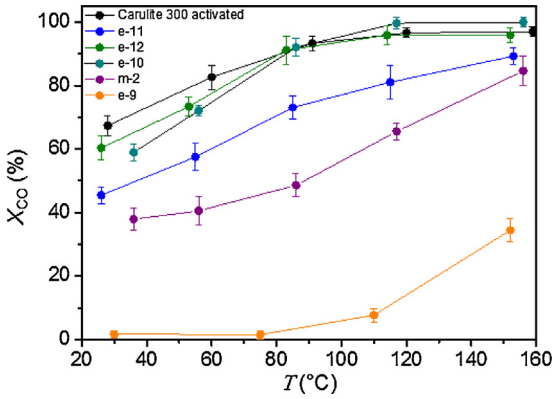

Fig. 4. Conversion of CO versus temperature for in house synthesised Mn(II)-2-ethylhexanoate samples e-10 to e-12, microemulsion derived sample m-2 and phosphorus contaminated sample e-9 under dry conditions.

Results of investigating the long term stability of these samples at ambient conditions normalised with respect to their specific surface areas are plotted in Fig. 5 showing exceptionally high CO conversion rates for the FSP derived powders, outperforming the commercial catalyst by a factor of 2. Sample e-10 exhibited the most stable performance for the observed time span. Furthermore e-type samples exhibit a smaller dumping volume than Carulite 300 after densification, meaning less volume would be occupied by the active material in a respiratory filter.

Initial rates of conversion can be restored by purging with pure nitrogen at 300 °C for 10 min. During this step mainly carbon dioxide was observed desorbing from the catalystsí surfaces, suggesting

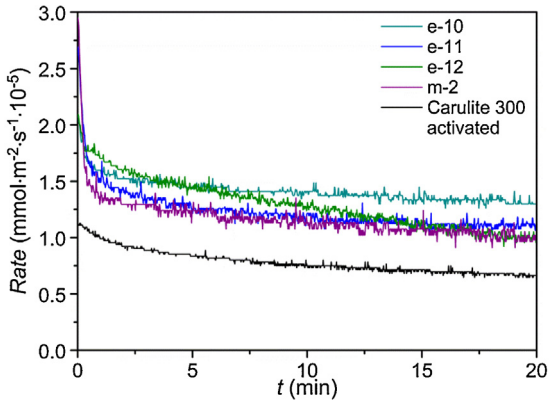

Fig. 5. CO oxidation long-term stability of the samples e-10 to e-12 and m-2 in comparison to the activated commercial reference material Carulite 300 at ambient temperature under dry conditions.

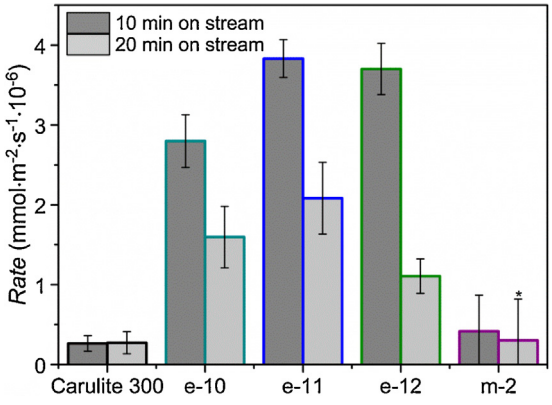

Fig. 6. Results of catalytic CO oxidation for the samples e-10 to e-12 and m-2 in comparison to the commercial reference material Carulite 300 under humid conditions (according to 75% humidity at 20 °C) at ambient temperature; *15 min on stream. Bar frame colours indicate the respective samples in Figs. 4, 5 and 7.

desorption of the reaction product is the rate limiting step at ambient temperature during the catalytic reaction.

For respiratory applications, humidity in air at ambient temperature is always a problem and hopcalite is known to rapidly deactivate due to water adsorption and blocking of the active sites [12]. Hence, huge volumes of upstream adsorbents restraining water vapour are required. Tests with gas streams containing 1.7 vol.% water vapour (corresponding to 75% RH at 20 °C or p_{vapour} = 17.63 hPa), resulted in fast deactivation for activated Carulite 300 and small CO conversion rates already after 5 min on stream, thus showing no stability against water vapour. In contrast, 2-ethylhexanoate based hopcalites showed CO conversion rates which were increased by one order of magnitude as compared to Carulite 300 even after 10 and 20 min on stream at ambient temperature (Fig. 6). The latter is a remarkable result and an important step towards humidity tolerant CO oxidation catalysts. At least volume for water vapour pre-adsorbents and for the active material could be reduced in respiratory filters and used for active components capturing additional toxic gases such as ammonia. Thus, broader possibilities for equipping multifunctional filters could be established.

3.2.3. Microemulsions

Microemulsion derived hopcalite particles showed intermediate conversion levels of CO at dry ambient conditions with around 35% for m-2 (Fig. 4). The long term conversion rates are comparable to the results of e-10, e-11 and e-12, outperforming Carulite 300,

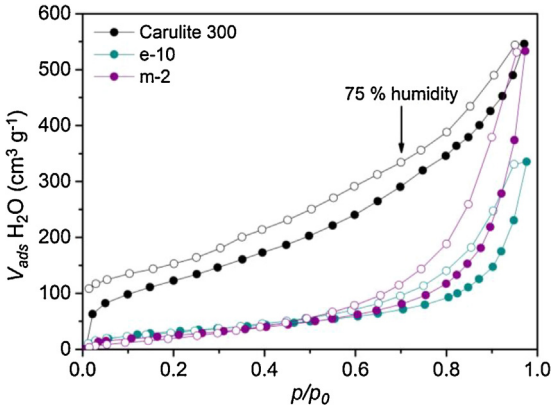

Fig. 7. Water sorption isotherms at 25 °C of samples e-10 and m-2 in comparison to the commercial reference material Carulite 300.

as well. Under humid conditions no significant activities remain for samples m-1 and m-2. Hence, no enhanced stability against water vapour was found for the microemulsion derived hopcalite particles (Fig. 6).

These remarkable results trigger the question: Where does the improved water stability of FSP-derived hopcalite originate from? Fig. 7 shows the water physisorption isotherms of Carulite 300, e-10 and m-2. Comparing these isotherms in the low pressure region ($p/p_0 < 0.1$) indicates extensive differences. Carulite 300 shows a much higher water uptake suggesting a more hydrophilic character as compared to e-10 and m-2. At the relevant level of humidity ($p/p_0 = 0.75$) the differences in water uptake are even more pronounced.

As Carulite 300 exhibits an overall specific surface area of 310 $m^2\,g^{-1}$, which is almost twice and thrice as high as compared to e-10 and m-2, respectively, statements on the relative hydrophobicity of those three samples are rather speculative. Thus, the ratio between the specific pore volumes at $p/p_0 = 0.75$ (according to 75% humidity at 20 °C) $V_{pore;0.75}(H_2O)$ and $V_{pore;0.75}(N_2)$ derived from water vapour and nitrogen physisorption isotherms, respectively, was calculated and we suggest to introduce the obtained value as a hydrophobicity index *HI*(75) (Eq. (3))

$$HI(75) = \frac{V_{pore;075}(H_2O)}{V_{pore;075}(N_2)} \quad (3)$$

A *HI*(75) close to 1.0 would account for a very hydrophilic character of the hopcalite powder. *HI*(75) « 1 would be characteristic for a rather hydrophobic material. For Carulite 300 *HI*(75) = 1.05 was found, while a value of 0.47 was calculated for e-10, illustrating the much less hydrophilic character of this sample. Sample m-2 exhibits an intermediate value of *HI*(75) = 0.87.

A possible reason for the decreased hydrophilic properties could be carbon located on the surface of the FSP-derived particles, which is most likely originating from incomplete combustion of the organic precursors and solvent components, thus forming a hydrophobic carbonaceous barrier. These carbon constituents are detectable, even though excess oxygen was always fed to the FSP process with $\varphi > 3.5$ for samples e-10 to e-12 and $\varphi > 1.5$ for m-1 and m-2, with

$$\Phi = \frac{\left[n(O_2)/n(\text{fuel})\right]_{real}}{\left[n(O_2)/n(\text{fuel})\right]_{stoich}} \quad (4)$$

Carbonaceous residues were quantified by elemental analysis and account for 0.24, 0.46 and 0.31 wt% in e-10, e-11 and e-12, respectively. m-2 contains only 0.11 wt% carbon, representing a possible reason for the different stabilities against water vapour in the catalytic oxidation of CO and the differences in *HI*(75) as com-

pared to e-10. After the catalytic tests (including activation at 300 °C in oxygen atmosphere for 1 h), carbonaceous residues of 0.15 wt% were found for e-10, while m-2 contained no carbon species, anymore, further indicating that carbon deposits are responsible for the improved water tolerance of 2-ethylhexanoate derived hopcalites.

Fig. S8 finally confirms a mean temperature stability of the carbonaceous barrier contained in sample e-10 under oxidative conditions. Two CO_2 peaks at 255 and 320 °C are observable together with water desorbing while releasing an exothermic heat of reaction. This suggests an aliphatic or aromatic character of the carbonaceous residues. No further desorbing CO_2 was detected up to a temperature of 500 °C during this experiment.

4. Conclusions

Hopcalite nanoparticle powders with tuneable compositions and particle sizes were synthesised using flame spray pyrolysis. Three different types of precursors, namely mixtures of Mn(II)-/Cu(II)-oleates, Mn(II)-/Cu(II)-2-ethylhexanoates and inversely microemulsified metal nitrates were evaluated concerning their ability to form contamination-free and catalytically active nanoparticles. Hopcalite powders synthesised from oleate mixtures gave $Cu_{1.5}Mn_{1.5}O_4$ and Mn_3O_4 with different mass fractions depending on the initial Mn:Cu-ratio. They were found to consist of up to 5 at% sodium, prohibiting effective conversion of carbon monoxide at room temperature. An initial molar ratio of Mn:Cu = 2 mol mol^{-1} was determined to achieve the highest conversion rates of CO at 150 °C.

Application of 2-ethylhexanoate mixtures resulted in nanoparticles with $Cu_{1.5}Mn_{1.5}O_4$ as the major crystalline phase besides small amounts of Mn_3O_4. A manganese rich X-ray amorphous phase was assumed to be present in the powders due to higher initial Mn:Cu-ratios of up to 2.8 mol mol^{-1}, contributing to the overall specific surface area of the powders. Spraying parameters and solvent composition were optimised to yield preferably separated nanocrystals of $Cu_{1.5}Mn_{1.5}O_4$ with mean diameters of 8 nm for the optimised synthesis conditions. After activation, these powders exhibited excellent conversion levels of CO at ambient temperatures comparable to those of the activated commercial hopcalite reference material Carulite 300.

While, a humidity of 75% at 20 °C caused a fast deactivation in the case of the commercial reference catalyst, hopcalite powders generated from the 2-ethylhexanoates offered much slower deactivation rates under humid conditions and ambient temperature. As a possible reason a hydrophobization originating from carbonaceous residues on the particles' surfaces may be the reason, as indicated by water sorption experiments, thus confirming increased hydrophobicity correlating well with carbon contents from elemental analyses.

A third type of precursor was prepared applying microemulsion techniques. Aqueous micelles served as hosts for dissolved manganese and copper nitrate and where dispersed in *n*-heptane, representing an efficient organic fuel for the combustion process. The latter is a versatile platform for the preparation of complex oxides. Nanocrystalline powders consisting mainly of $Cu_{1.5}Mn_{1.5}O_4$ and a minor portion of Mn_3O_4 with hopcalite crystallite sizes of about 11 nm in diameter were received. Their catalytic performance was in the same range as compared to the 2-ethylhexanoate derived powders, concerning conversion rates normalised to the powders' specific surface areas under dry conditions at ambient temperature. Humidity caused a fast deactivation in those powders, which was comparable to that of Carulite 300 and is probably caused by lower amounts of carbon residues with only one third of the carbon content found in 2-ethylhexanoates derived FSP-hopcalites.

Summarizing, an alternative preparation route towards highly active hopcalite nanoparticles was presented, using few time and resources saving preparation steps and alkali ion free precursor formulation. The synthesised hopcalite nanopowders are an important step towards the development of eco-efficient air purification systems in highly polluted areas and may find applications in respiratory filters, air conditioning as well as in the automotive industry for the selective oxidation of Pt-anode poisoning CO contained in the feedstock for fuel cells.

Acknowledgements

We would like to thank Dr Gudrun Auffermann (MPI for Chemical Physics of Solids, Dresden, Germany) for conducting elemental analyses. Alexander Weiz (Department of Inorganic Chemistry II, Dresden University of Technology, Dresden, Germany) is acknowledged for his support with preparing STEM micrographs. We would also like to thank the German Federal Ministry of Education and Research (BMBF) for financial support (03X0126C).

Appendix A. Supplementary data

Supplementary data associated with this article can be found, in the online version, at http://dx.doi.org/10.1016/j.apcatb.2015.11.008.

References

[1] T. Gerhardt, M. Göthert, G. Malorny, H. Wilke, Int. Arch. Für Arbeitsmed. 28 (1971) 127–140.
[2] J. Saavedra, C. Powell, B. Panthi, C.J. Pursell, B.D. Chandler, J. Catal. 307 (2013) 37–47.
[3] X. Xie, Y. Li, Z.-Q. Liu, M. Haruta, W. Shen, Nature 458 (2009) 746–749.
[4] M. Haruta, N. Yamada, T. Kobayashi, S. Iijima, J. Catal. 115 (1989) 301–309.
[5] A. Bliss, J. Am. Chem. Soc. 77 (1955) 5773–5780.
[6] M. Krämer, T. Schmidt, K. Stöwe, W.F. Maier, Appl. Catal. Gen. 302 (2006) 257–263.
[7] Z.-R. Tang, C.D. Jones, J.K.W. Aldridge, T.E. Davies, J.K. Bartley, A.F. Carley, et al., ChemCatChem 1 (2009) 247–251.
[8] E.C. Njagi, C.-H. Chen, H. Genuino, H. Galindo, H. Huang, S.L. Suib, Appl. Catal. B Environ. 99 (2010) 103–110.
[9] G.J. Hutchings, A.A. Mirzaei, R.W. Joyner, M.R.H. Siddiqui, S.H. Taylor, Catal. Lett. 42 (1996) 21–24.
[10] A.A. Mirzaei, H.R. Shaterian, R.W. Joyner, M. Stockenhuber, S.H. Taylor, G.J. Hutchings, Catal. Commun. 4 (2003) 17–20.
[11] G.J. Hutchings, A.A. Mirzaei, R.W. Joyner, M.R.H. Siddiqui, S.H. Taylor, Appl. Catal. Gen. 166 (1998) 143–152.
[12] C.-H. Chen, E.C. Njagi, S.-P. Sun, H. Genuino, B. Hu, S.L. Suib, Chem. Mater. 22 (2010) 3313–3315.
[13] C.R. Bickmore, K.F. Waldner, D.R. Treadwell, R.M. Laine, J. Am. Ceram. Soc. 79 (1996) 1419–1423.
[14] M. Sokolowski, A. Sokolowska, A. Michalski, B. Gokieli, J. Aerosol Sci. 8 (1977) 219–230.
[15] W.Y. Teoh, R. Amal, L. Mädler, Nanoscale 2 (2010) 1324.
[16] T. Biemelt, K. Wegner, J. Teichert, S. Kaskel, Chem. Commun. 51 (2015) 5872–5875.
[17] J. Henle, P. Simon, A. Frenzel, S. Scholz, S. Kaskel, Chem. Mater. 19 (2007) 366–373.
[18] K.S.W. Sing, Pure Appl. Chem. 54 (1982) 2201–2218.
[19] H.K. Kammler, L. Mädler, S.E. Pratsinis, Chem. Eng. Technol. 24 (2001) 583–596.
[20] L. Mädler, H.K. Kammler, R. Mueller, S.E. Pratsinis, J. Aerosol Sci. 33 (2002) 369–389.
[21] R.E. Vandenberghe, G.G. Robbrecht, V.A.M. Brabers, Mater. Res. Bull. 8 (1973) 571–579.
[22] R. Strobel, S.E. Pratsinis, J. Mater. Chem. 17 (2007) 4743.